An optical method for studies on bubble behaviour in turbulent flows

by

D. Bröder and M. Sommerfeld

Institut für Verfahrenstechnik / Mechanische Verfahrenstechnik
Fachbereich Ingenieurwissenschaften
Martin-Luther-Universität Halle-Wittenberg
D-06099 Halle (Saale), Germany
Email: martin.sommerfeld@iw.uni-halle.de
Key-words: PIV, PTV, Two-phase flow, bubbly flow

Abstract

In order to allow more reliable modelling of coalescence processes in turbulent bubbly flows, detailed experiments in a double loop reactor were performed. The range of bubble diameters considered in the measurements was about 2 to 4 mm. Narrow, essentially monomodal bubble size distributions were created by capillary aerators. For simultaneous measurements of bubble size, bubble velocity and liquid velocity a combined system of PIV and PTV was developed and applied. In order to perform measurements of the liquid velocities the flow was seeded with polyamide tracer particles with mean averaged diameter of 50 µm.

A background illumination was realised by using an array of 91 LED's with a size of 100 by 75 mm. A CCD camera with a macro camera optics was used to record images of tracers and bubbles. Because of the small depth of field of the macro camera optics (< 4 mm) it was possible to discriminate between bubbles and tracer particles inside and outside of the camera's focus plane by the gradient of grey values. Sharply depicted objects in the focus plane have high gradients while blurred objects out of focus have low gradients of grey values. A set of digital image filters was used to perform the phase discrimination between bubbles and tracer particles. The resulting images were evaluated by two different imaging velocity techniques. In case of the bubbles the Particle Tracking Velocimetry (PTV) was used to determine bubble sizes and velocities and for the liquid velocities the images of tracer particles were evaluated by the Particle Image Velocimetry (PIV).

By recording and evaluating a large number of images it was possible to determine bubble size distributions and mean but also fluctuating velocities for both phases in all areas of the described apparatus. The spatial changes of the bubble size distribution due to the influence of bubble coalescence was analysed and coalescence rates were calculated from this information.

1. INTRODUCTION

In order to analyse bubbly flows several optical measurement techniques have been developed and applied during the last years. These are mainly phase-Doppler and laser-Doppler velocimetry, acoustic measurement techniques, particle image velocimetry (PIV), particle tracking velocimetry (PTV), and holographic techniques. Many of these analysing methods register only the properties of one phase. A combination of more than one method is necessary to characterise the properties of both phases. Simultaneous measurements of both phases are rarely possible and limited to simple experimental arrangements. Many highly developed techniques like phase- and laser-Doppler velocimetry provide precise information of bubble sizes and velocities of bubbles and liquid. But low data rates caused by low bubble number concentrations and velocities and light absorption give rise to very long sampling times per measurement point. This means that the measurement of a complete flow map in an apparatus, which is necessary for comparisons with numerical simulations, is hardly possible because of long measurement periods. Additionally, phase-Doppler velocimetry is limited in its application by the bubble size. Because of their non-spherical shape, bubbles with more than about 1 mm diameter cannot be sized correctly with PDA (Tassin & Nikitopoulos 1995). For a 1 mm ellipsoidal bubble in water the ratio between the length of the main axes is 1.15 (Duineveld 1994). This means consistency errors in determining the phase differences of Doppler bursts and hence considerable errors in determining the size of these bubbles. Modern camera optical measurement techniques like PIV and PTV are able to realise complete planes of a flow and together with methods of digital image processing techniques it is possible to provide velocities of both phases and also information about size, shape and position of bubbles.

A big problem for the application of standard PIV to bubbly flows is the strong absorption of the penetrating laser light sheet by scattering on the surface of the bubbles at higher void fractions. Because the intensity of the light scattered by bubbles is several decades larger than the scattering intensity of conventional tracer particles, many investigators used fluorescing tracer particles and a phase separation by the different wavelengths of the light source and the fluorescing dye in the tracers. But Diaz & Riethmuller (1998) have shown that the bubble contour cannot be obtained from PIV images because of optical effects which occur at the bubble interface when it crosses a laser light sheet and therefore a supplementary CCD-camera is required to acquire bubble contour images (Bröder and Sommerfeld 2000, 2002).

The application of two and more cameras and light sources cause quite extensive experimental set-ups and time consuming measurement and evaluation procedures. A rather reasonable technique for the simultaneous measurement of the bubble sizes and the velocities of both phases was proposed by Borchers et al. (1999). One CCD-camera with a macro camera optics of a small depth of field acquired background illuminated images of bubbles and tracer particles. The phase separation was performed by some object recognition and the velocities of bubbles and the liquid phase were evaluated by an algorithm based on the principles of the PTV.

As the evaluation method of Borchers et al. (1999) is quite time consuming, a new more efficient system with the ability for online measurements was developed and applied to analyse the hydrodynamic interaction and coalescence in a laboratory airlift reactor.

2. EXPERIMENTS

2.1 Test Facility

The experimental facility was a rectangular container of Plexiglas with the inner dimensions 2300 x 300 x 100 mm. The apparatus (Fig. 1) was aerated from the middle part by two capillary aerators and each of these aerators was connected to a single flux controller. The capillaries had a diameter of 0.4 and 0.6 mm and each aerator consisted of 50 capillaries. Between the aerators a splitter plate was installed which kept the two bubbly flows separated up to a height of 1100 mm from the bottom of the container. Downstream of the end of the splitter plate the different bubbly flows were mixed so that the two bubble populations could interact. Two more plates separated the up comer in the middle of the apparatus from the two outer downcomer channels. Two weirs in the upper part of the apparatus were used to reduce the liquid velocity in the two loops and to control the turbulence intensity in the mixing zone. As the internal water level would decrease during long measurements periods, it was kept constant by electronic level controller.

A CCD-camera and a pulsed LED array as light source were mounted on a CNC traversing system allowing to perform fully automated measurements at all positions inside the airlift facility. This traversing system was also used as a camera lifter to follow rising bubbles with a high-speed camera. All components of the measurement system and the CNC traverse system were controlled by the image processing PC (Intel Pentium III 700 MHz) to allow fully automated online measurements for both phases of the bubbly flow. The synchronisation of the CCD-camera and the pulsed LED-array, as well as the pulse duration and the time delay between the pulses were performed by a timer card, which was also installed in the image processing PC. The processing time for filtering a double image, detecting the bubble and performing a PTV took around 1 s, while the processing time for filtering and performing a PIV for the liquid phase took around 5 s. The typical overall measurement time for a combined measurement of both phases at 5 measurement positions was 12 to 15 h.

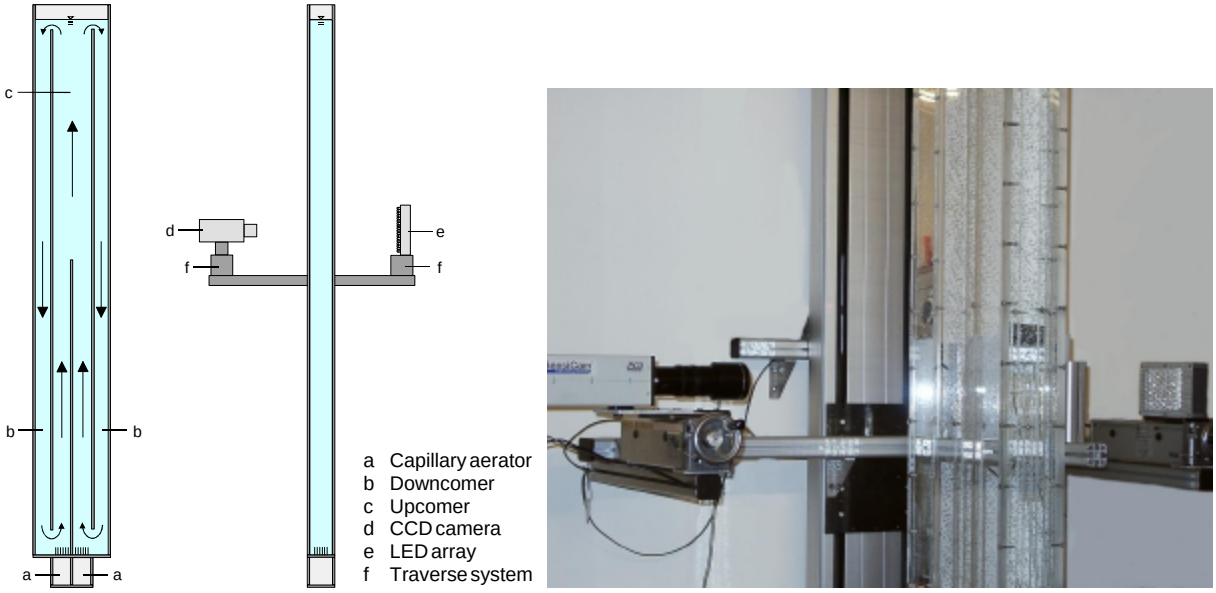

Fig. 1: Airlift facility with CCD camera, pulsed LED array and CNC traverse system.

2.2 Image acquisition

The images of the two-phase flow were acquired by a double shutter camera (PCO SensiCam) which allowed to acquire two image with a resolution of 1280 by 1024 pixel within a very short time delay. The images were exposed in a background illuminated mode using a pulsed LED-array consisting of 91 high performance LED's with a total area of 100 x 75 mm. The typical duration of the light pulses was 200 µs, while the time delay between two singly exposed pictures was adjusted to the local flow velocity in a range from 1 to 3 ms. The images were transferred in a digital way from the CCD-camera to the controlling and image processing PC. The evaluation of the images and all controlling tasks were performed by an in-house developed software. In a first image processing step the images were transformed from the cameras 12 bit format to a 8 bit format grey value image. Therefore, the histogram of greyvalue of each images was analysed and from this histogram a contrast optimised lookup table for the transformation was created.

In order to allow measurements of the liquid velocity fields the flow was seeded with polyamide tracer particles with a mean diameter of 50 µm and a density of 1050 kg/m^3. The phase discrimination between bubbles and tracer particles was performed in the evaluation procedure using digital image filters. Because of the small depth of field of the macro camera optics (< 4 mm) it was possible to discriminate also between bubbles and tracer particles inside and outside of the camera's depth of focus by the gradient of grey values. Sharply depicted objects in the focus have high gradients, while blurred objects out of focus have low gradients of grey values.

2.3 Bubble detection

In order to perform an automatic bubble detection, the recorded images needed to be prepared by a set of digital filters before an object recognition for the bubbles was applied. The tracer particles and small scale noise was deleted from the images by a non-linear 5x5 median filter and the gradient $S(x,y)$ of the contours of sharply depicted bubble was calculated by an edge-detecting Sobel filter with the convolution kernels $S_X(x,y)$ and $S_Y(x,y)$:

$$S(x,y) = \sqrt{S_X^2(x,y) + S_Y^2(x,y)}$$

$S_X(x,y)$:

-1	0	1
-2	0	2
-1	0	1

$S_Y(x,y)$:

-1	-2	-1
0	0	0
1	2	1

During the object recognition for the bubbles the gradient of the grey values at the contours of the bubbles, i.e. the sharpness, was used as a criteria for the validation. Additionally, the continuity of the contours was used as a validation criteria. As overlapping bubbles in the images resulted in incomplete contours, it was necessary to reconstruct missing contour points by a cubic spline interpolation. The information of the contour points of the bubbles were used to calculate projection areas, centroids, area equivalent diameters and the longest and shortest chord length. An example of a bubble detection algorithmn is given in Fig. 2.

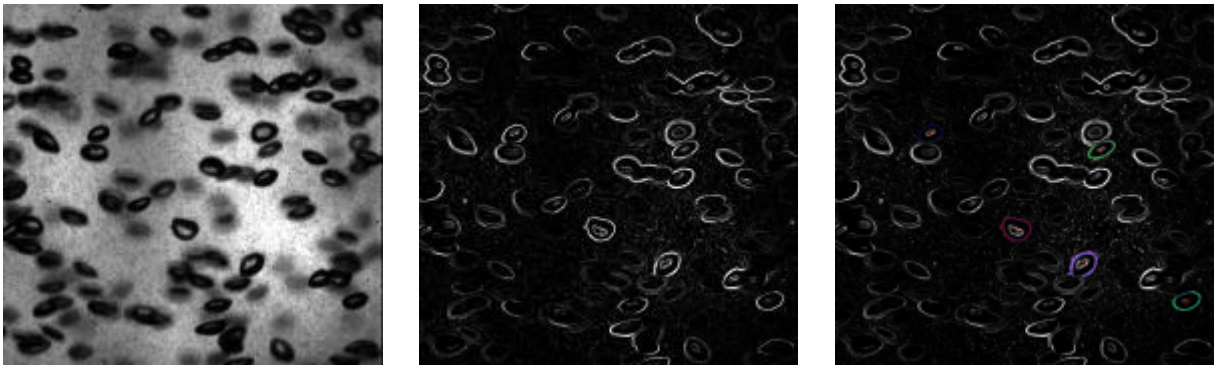

a) b) c)

Fig.2: Example of the bubble detection algorithmn.
a) Original background illuminated image of the bubbly flow seeded with tracer particles.
b) Image filtered with a median filter and a Sobel filter.
c) Only sharply depicted bubbles (coloured ones) are validated.

2.4 Estimation of bubble volumes and coalescence rates

For analysis of coalescence processes the knowledge of the bubble volumes is required. Most of the investigations performed with cameras acquire only one projection of the bubbles, which allows to determine a number of geometrical parameters like projection areas, chord lengths, perimeter and orientation of the main axis, but no precise determination of the bubble volumes is possible. Accurate bubble volume measurements could be realized by two perpendicular projections to gain additional information about the spatial extent of a bubble. But a simultaneous registration of two projections of one bubble is unlikely to occur even at low void fraction and impossible to realise in the described apparatus for void fractions higher than 4 %. Therefore, the information of only one projection provides an estimation of the bubble volume and the accuracy of the volume determination will be better for small rigid and spherical bubbles than for large bubbles with strong shape oscillations.

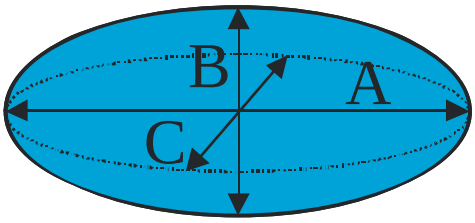

Fig. 3: Oblate spheroid with main axes

The simplest way to estimate the bubble volume V_B is to determine a bubble diameter D_A which is area equivalent to the projection area A_{Pro} of a detected bubble:

$$A_{\mathrm{Pro}} = \frac{p}{4} AB = \frac{p}{4} D_A^{\,2} \tag{1}$$

The bubble volume corresponds to the volume of a sphere with this area equivalent diameter. However, bubbles with larger area equivalent diameters than 2 mm have a ratio between the length of the major axis larger than 2 (Duineveld 1994) and differ considerably from a sphere. These bubbles can be described as oblate spheroids (Fig. 3):

$$V_{Sph} = \frac{p}{6} ABC \tag{2}$$

Both horizontal major axes A and C are approximately equal and larger than the vertical major axis B. By substitution of the missing major axis C with the longest chord length of the bubble contour A, an estimation of the bubble volume V_B is provided by the following equation:

$$V_B = \frac{p}{6} A^2 B = \frac{p}{6} D_A^2 * A \tag{3}$$

Evaluations of high speed recordings for bubbles of an area equivalent diameter D_A = 3.8 mm have shown a relative deviation of 12 % for the volume determination following equation (3) and a relative deviation of 16 % following equation (2).

The present investigations were performed in water purified by a reverse osmosis purification system. The system water/air was analysed by many authors (Oolman and Blanch 1986, Zahradník et al. 1995) with regard to coalescence behaviour in a stagnant liquid. For the investigated bubble size and the low turbulence intensity in the apparatus, the occurrence of bubble break-up can be neglected. Therefore, changes of the bubble size were caused by coalescence of bubbles and the change of the hydrostatic pressure along the rise of bubbles. In order to quantify the coalescence, the properties of the bubbles and the continuous phase were measured at 5 horizontal profiles along one of the risers up to the end of the splitter plate. The coalescence rate G_T was determined from the change of the bubble volume distribution between two measurement profiles following Prince und Blanch (1990):

$$\Gamma_T = \frac{c_B}{t_r} \frac{V_{gc}}{V_{gT}} \frac{\overline{V}_b}{\overline{V}_{bc}} \tag{4}$$

The bubble concentration c_B was calculated with the mean bubble velocity of the profiles, the bubble volume distribution and the superficial gas velocity. The residence time t_r was also calculated by the mean bubble velocity of the profiles and the distance between the measurement profiles. The coalesced volume V_{gc} corresponds to the positive integral area of the difference between two volume distributions (Fig. 4). The mean bubble volume of coalesced bubbles $\overline{V}_{bc}$ is also calculated from this area, while the mean bubble volume $\overline{V}_b$ results from the total volume of gas V_{gT}. Bubble volumes from different measurement positions have to be corrected by the ideal gas law because of the volume expansion due to the change of the hydrostatic pressure.

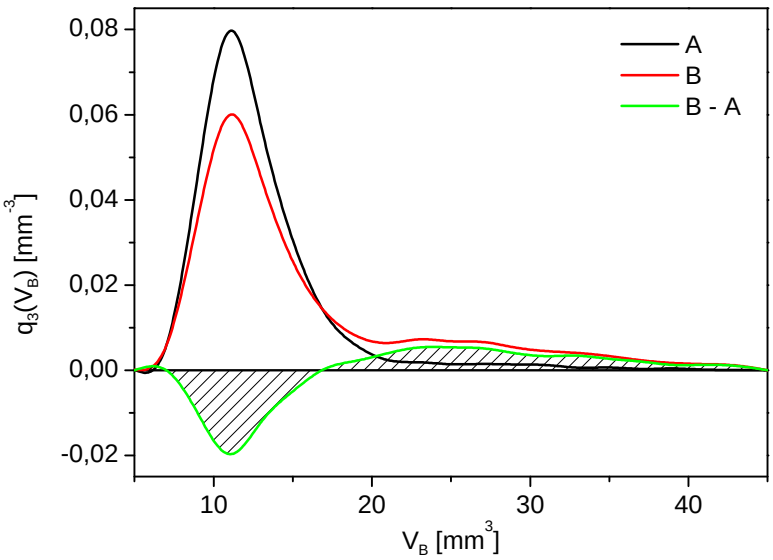

Fig. 4: Determination of the coalescence rate from the difference of two volume distributions. Distribution A is the basic distribution, distribution B contains bubbles after coalescence. Distribution B-A is the difference between the distributions A and B.

2.5 Bubble velocity measurements (PTV)

The velocities of the bubbles were determined by the application of the Particle Tracking Velocimetry (PTV) and the described bubble detection algorithm for two consecutive images. Corresponding bubble pairs were found by the criteria of overlapping bubble contours and the closest neighbour in direction of the bubble rise. The bubble velocity was calculated from the translation of the centroids of the bubbles within both images, the

time delay and the magnification factor. The translations of the centroids of the bubbles and the information extracted by the bubble detection were stored together for later post-processing of the data.

2.6 Liquid velocity measurements (PIV)

The velocities of the continuous phase were determined by the application of the Particle Image Velocimetry (PIV) to the extracted images of the tracer particles. This extraction was performed with an edge filter proposed by Marr and Hildreth (1980) which is often called Laplacian of Gaussian (LoG). The fundamental characteristics of the LoG edge detector are the combination of a smoothing Gaussian filter and an enhancement step which is a Laplacian second derivative in two dimensions. The output of the LoG operator *L(x,y)* is obtained by the convolution operation of a Gaussian filter *G(x,y)* applied to the image matrix *f(x,y)*:

$$L(x,y) = \nabla^2[G(x,y) * f(x,y)] \tag{5}$$

Using the derivative rule for convolution:

$$L(x,y) = [\nabla^2 G(x,y)] * f(x,y) \tag{6}$$

where

$$\nabla^2 G(x,y) = \left(\frac{x^2 + y^2 - 2s^2}{s^4} \right) e^{-\frac{(x^2+y^2)}{2s^2}} \tag{7}$$

is commonly called the Mexican hat operator (Fig. 5). The standard deviation σ was fitted to the images of the tracer particles to optimise the function of the LoG filter.

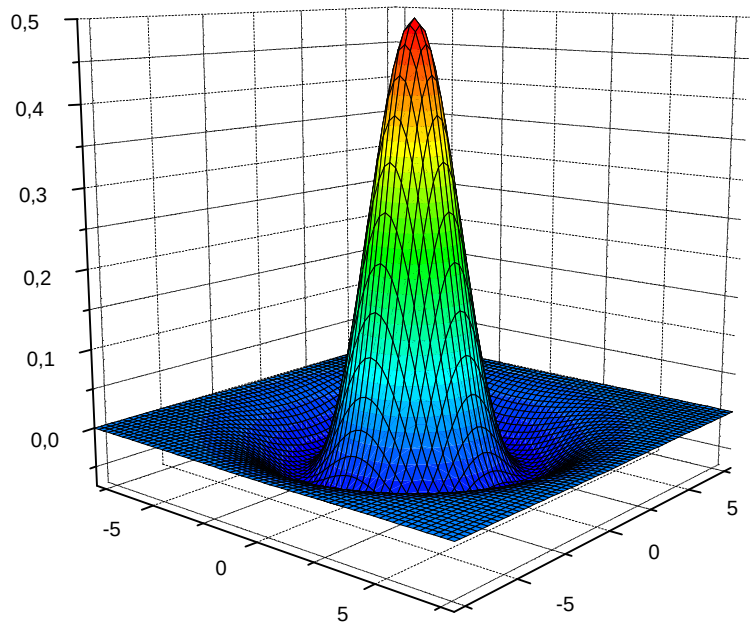

Fig. 5: The inverted Laplacian of Gaussian function (Mexican hat operator) for s=2 in two dimensions.

For a further optimisation of the LoG filter to the images of the tracer particles, it was necessary to seed the flow with narrow size distributed particles. Therefore, the tracer particles were sieved and only the fraction in the range of 40 to 60 µm was used for seeding the bubbly flow. After the application of the LoG edge detector the images of the tracer particles but also the contours of sharply depicted bubbles were kept inside the images. Therefore, an additionally image operation was used to remove these bubble contours. The schematic diagram of the filter structure is given in Fig. 6. A median filtered image was created which contained only large objects like bubble contours but no tracer particles (Image C). This median filtered image with it's bubble contours was subtracted from the image filtered by the LoG edge detector (Image B) and so the resulting image (Image D) was prepared for the PIV evaluation containing only the tracer particles.

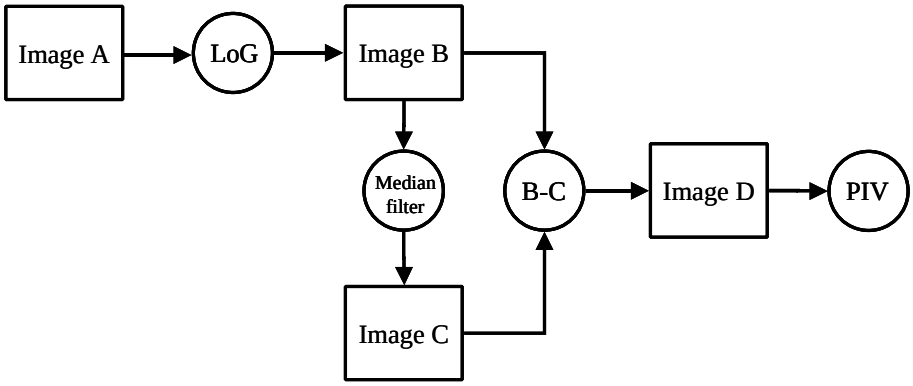

Fig. 6: Schematic diagram of the filter structure for the phase discrimination of the liquid by extracting the images of tracer particles from the pictures of the two-phase flow.

The evaluation of the filtered images was performed by a PIV with iterative refinement of the interrogation areas following an approach of Scarano et al. (1999). The cross correlation was based on the Minimum Absolute Difference Method (MAD) and the Minimum Quadratic Difference Method (MQD) developed by Gui et al. (1997). The first two iterative steps were performed with the fast MAD and an interrogation area size of 128 x 128 pixel in case of the first step and 64 x 64 pixel for the second step. As the sub pixel accuracy of the MAD is less than that of the slower MQD, only the last iterative step was performed by the more accurate MQD. The interrogation area size of the last step was 40 x 40 pixel which corresponds to an area of 1.95 x 1.95 mm. Further details about the applied PIV can be found in Bröder and Sommerfeld (2002). By recording and evaluating a huge number of images it was possible to determine instantaneous (Fig. 7) but also mean and fluctuating velocities fields for the continuous phase within the bubble swarm in all areas of the described apparatus.

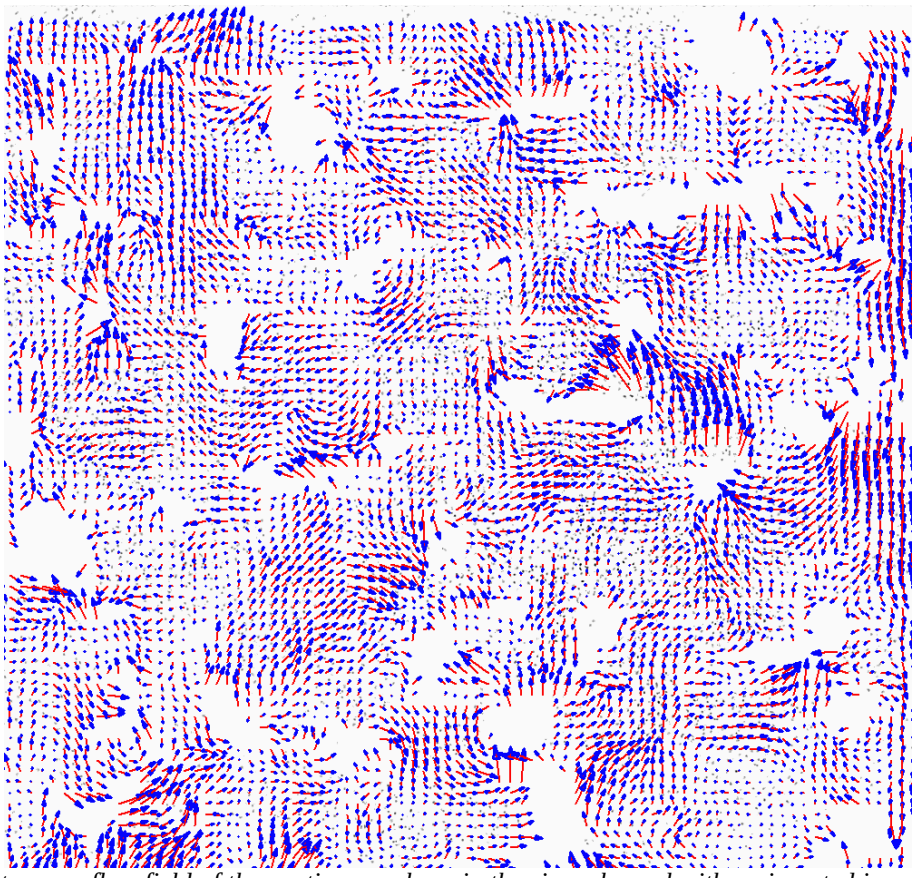

Fig. 7: Instantaneous flow field of the continuous phase in the riser channel with an inverted image of extracted tracer particles in the background. Mean velocities of the vector field have been subtracted to visualise the turbulent fluctuation. Missing vectors are caused by shadows of bubbles and low seeding density. Void fraction 0.73 %, measurement position: 800 mm above the entry of the riser channel, dimension 40 x 40 mm.

3. RESULTS

3.1 Profiles of the flow

All presented measurements were done in the one of both risers up to the end of the splitter plate. Therefore, the measurements are restricted to interactions of approximate equal sized bubbles and will be used as initial conditions for further measurements in the area above the splitter plate where interactions of different sized bubbles shall be investigated. The main operating conditions of the measurements are summarized in Table 1.

Gas volume flow [l/h]	Superficial gas velocity [cm/s]	$\overline{V}_b$ at h=0 [mm^3]	Void fraction at h=800 mm [%]
40	0,22	14,6	0,73
60	0,33	15,1	1,33
80	0,44	14,6	1,75

Table 1: Parameters of the measurements.

The profiles of the mean and fluctuating velocities of the liquid were determined by averaging the information of 500 PIV vector fields per profile. The measurements of the velocities of the continuous phase showed up to the height of 800 mm no completely developed flow, because of the short length of the riser channel. This is shown by the velocity profiles for three different void fractions, presented in Fig. 8, which are not symmetric. The liquid velocity increases with rising gas volume flow, due to the increasing energy input into the apparatus. Also the fluctuating velocities increase slightly with the gas void fraction and show the anisotropic character of the pseudo-turbulent bubbly flow.

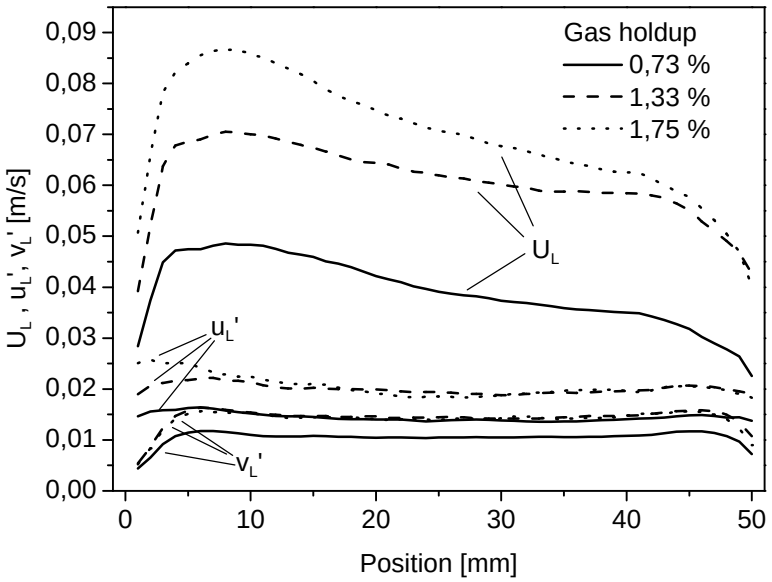

Fig. 8: Profiles of the mean and fluctuating velocities of the liquid for different void fractions measured at a height of 800 mm above the entry of the riser channel.

The profiles of the mean bubble velocities in Fig. 9 are similar to the profiles of the mean liquid velocities in Fig. 8. Therefore, the relative velocities in Fig. 10 are approximately constant across the channel width with some exception for the regions close to the walls. With increasing void fraction the relative velocity between both phases is slightly decreasing. The velocity fluctuations of the bubbles in vertical and horizontal direction are strongly anisotropic. The reason for the large horizontal fluctuations are the strong horizontal oscillations of the bubbles with a size in the range from 2 to 4 mm. This behaviour is quite different to the fluctuating velocities of the liquid as the horizontal components are smaller.

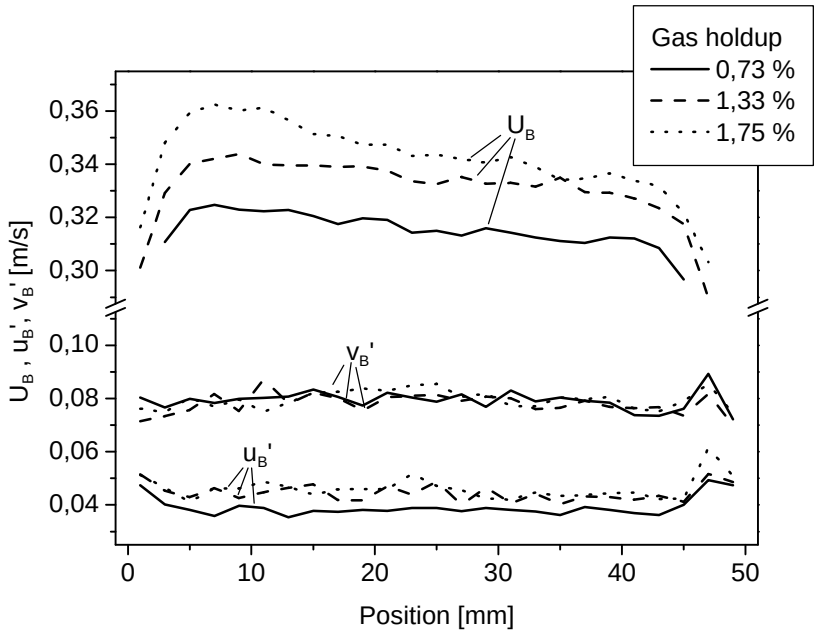

Fig. 9: Profiles of the mean and fluctuating velocities of the bubbles for different void fractions measured at a height of 800 mm above the entry of the riser channel.

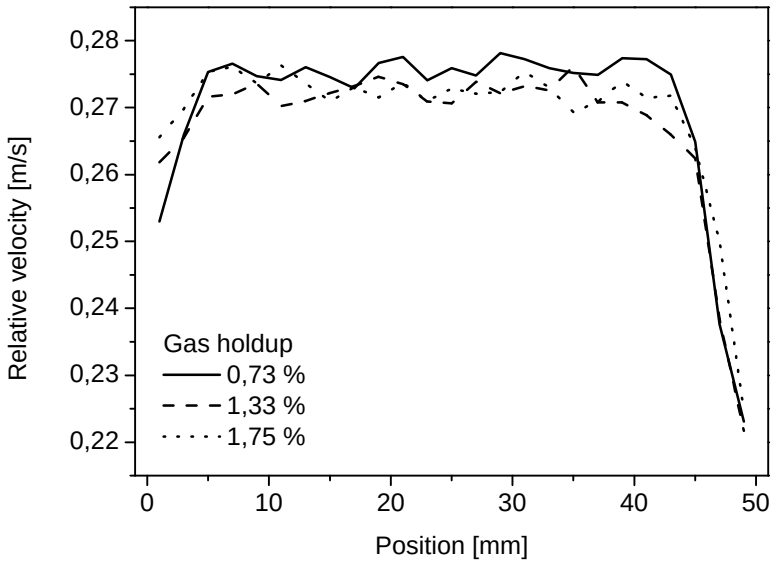

Fig. 10: Profiles of relative velocities between bubbles and liquid for different void fractions measured at a height of 800 mm above the entry of the riser channel.

3.2 Coalescence rates

For the determination of the coalescence rate from the change of the bubble volume distribution along the riser channel, at least 30000 bubbles had to be collected per measurement plane. The change of the bubble volume distribution due to coalescence for the case of 0.73 % void fraction obtained over the entire channel width and a height of 40 mm is showed in Fig. 11. The basic bubble population has a peak at about 12 mm^3 which decreases with the height of the measurement position, while a second peak with twice the volume of the basic population grows at approximately 25 mm^3. Thereby, the volume distribution becomes more and more bimodal. The coalescence rates for the operating conditions described in 3.1 are showed in Fig. 12. The coalescence rates of course increase with rising void fraction due to the increasing bubble concentration. However, at the higher void

fractions the coalescence rates decrease with the height of the measurement position, as a larger fraction of the basic population has coalesced already in the range of the lower measurement positions.

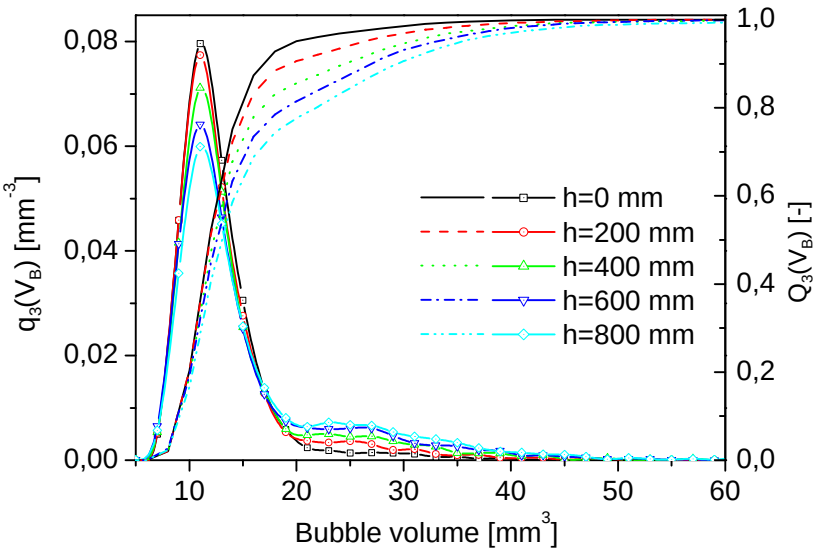

Fig. 11: Changes of the bubble volume distribution in one of the riser channels for a void fraction of 0.73 %.

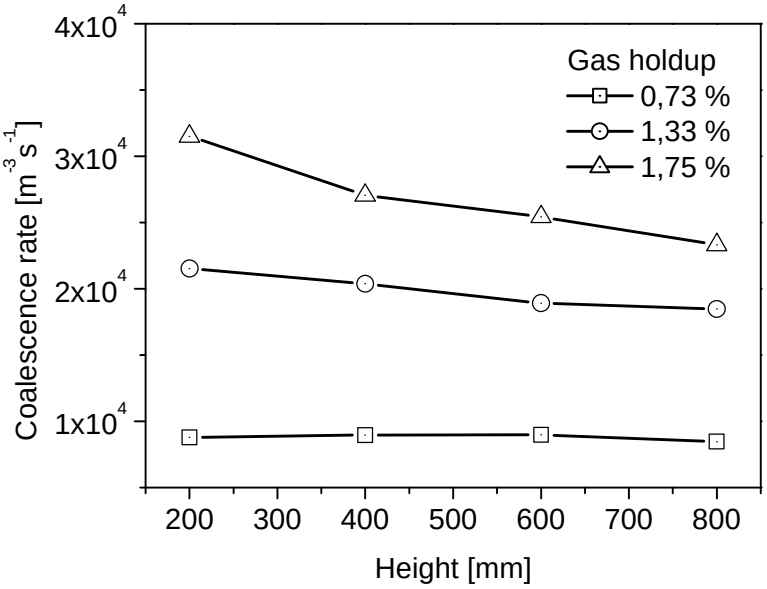

Fig. 12: Coalescence rates in a riser channel for different void fractions.

CONCLUSIONS

The described measurement system combining imaging PIV and PTV is able to acquire a lot of important parameters in a two-phase flow. Therefore, it provides a potential to create detailed datasets for validating numerical simulations. Additionally, further analysis of the hydrodynamic interactions of bubbles in a swarm were possible. The coalescence rates for monosized bubbles were determined for different void fractions. In future investigations the applicability of the system will be applied for different operating modes and especially for higher void fractions. The simultaneous measurements of bubble size, bubble velocity and liquid velocity allow a sophisticated post-processing of the collected data in order to analyse more interesting parameters like collision rate and correlations between the fluctuating components of the phases.

ACKNOWLEDGEMENTS

The financial support of the present studies by the Deutsche Forschungsgemeinschaft under contract number SO 204/19 is gratefully acknowledged.

REFERENCES

Borchers, O., Busch, C. and Eigenberger G. (1999). „Analyse der Hydrodynamik in Blasenströmungen mit einer Bildverarbeitungsmethode“, Proceedings of the 2th Workshop on Measurement Techniques for Steady and Transient Multiphase Flows, Rossendorf (Dresden), Germany.

Bröder, D. and Sommerfeld, M. (2000) “A PIV/PTV system for analysing turbulent bubbly flows”, Proceedings of the 10th International Symposium Application of Laser Techniques to Fluid Mechanics, Lisbon, Paper 10.1.

Bröder, D. and Sommerfeld, M. (2001) “Experimental studies of the hydrodynamics in a bubble column by an imaging PIV/PTV-system”, Proceedings of 4th International Symposium on Particle Image Velocimetry, Göttingen, Germany, September 17-19.

Bröder, D. and Sommerfeld, M. (2002) “An advanced LIF-PLV system for analysing the hydrodynamics in a laboratory bubble column at higher void fractions”, Experiments in Fluids, In Print.

Diaz, I. and Riethmuller, M.L. (1998). “PIV in two-phase flows: Simultaneous bubble sizing and liquid velocity measurements.” 9th Int. Sym. on Applications of Laser Techniques to Fluid Mechanics, Lisbon, Portugal.

Duineveld, P. C. (1994). “Bouncing and coalescence of two bubbles in water”, Ph.D. Thesis, University of Twente-Netherlands: ISBN 90-9007541-0.

Gui, L., Lindken, R. and Merzkirch, W. (1997) “Phase-separated PIV Measurements of the Flow Around systems of Bubbles Rising in Water”, ASME-FEDSM97-3103.

Gui, L., Merzkirch, W. (1997) “A fast mask technique for the phase-separated evaluation of two phase PIV recordings”, Proceedings of the 7th International Conference on Laser Anemometry, Karlsruhe, Germany, September 8-11.

Marr, D. and Hildreth, E. (1980). “Theory of edge detection”, Proceedings of the Royal Society of London, B 207, pp. 187-217.

Oolman, T. O. and Blanch, H. W. (1986) “Bubble Coalescence in Stagnant Liquids”, Chem. Eng. Comm., Vol. 43, pp. 237-261.

Prince, M. J. and Blanch, H. W. (1990) “Bubble Coalescence and Break-Up in Air-Sparged Bubble Columns”, AIChE Journal, 36, pp. 1485-1499.

Scarano, F. and Riethmuller, M. L. (1999) “Iterative multigrid approach in PIV Image processing with discrete window offset”, Experiments in Fluids, Vol.26, pp. 513-523.

Tassin, A.L. and Nikitopoulos, D.E. (1995) “Non-intrusive measurements of bubble size and velocity”, Experiments in Fluids, Vol. 19, pp. 121-132.

Zahradník, J., Fialova, M., Kaštánek, F., Green, K.D. and Thomas, N.H. (1995). “Effect of Electrolytes on Bubble Coalescence and Gas Holdup”, Trans IchemE, Vol.73, Part A.